JOURNAL OF SPACECRAFT AND ROCKETS
Vol. 44, No. 6, November–December 2007

Measurement of In-Plane Motion of Thin-Film Structures Using Videogrammetry

Jack Leifer*
Trinity University, San Antonio, Texas 78212
and
Jonathan T. Black,† Suzanne Weaver Smith,‡ Ning Ma,§ and Janet K. Lumpp¶
University of Kentucky, Lexington, Kentucky 40506

DOI: 10.2514/1.25566

An electrodynamic shaker was used to apply a 1-Hz, 1.5-mm-amplitude, in-plane harmonic excitation to a thin-film gossamer material mounted in an aluminum fixture. Using a two-camera videogrammetric setup that simultaneously imaged the test article at 75 frames per second (per camera), the *x*, *y*, and *z* motion components of two points on the thin film (F1 and F2) as well as of two points on the aluminum holder (R1 and R2) were tracked for a total of 4 s. The in-plane motion components of each tracked point closely corresponded to the excitation provided by the shaker. The presence of modally induced in-plane film deformation was confirmed by tracking the change in distance between points F1 and F2. The standard deviation of the value of the measured distance between these two points was found to be about 57 μm. This value was well above the noise floor for this measurement, 11 μm, experimentally determined by calculating the standard deviation of the measured distance between points R1 and R2 on the aluminum film holder, which was considered to be rigid and hence was not expected to undergo in-plane deformation.

I. Introduction

PRECISION thin-film structures for space applications must maintain their shape in an environment full of dynamic disturbances. These structures, which include solar sails proposed for future missions,** as well as the thermal shielding elements for the James Webb Space Telescope†† (Fig. 1), resemble cellophane or Mylar and typically consist of a thin polymer-film base material with an additional metal layer adhered to the surface for reflectivity. Their low mass, coupled with the ability to deploy to full size from a compact launch configuration, offers an ultralightweight solution to the challenge of launching large spacecraft. State-of-the-art approaches for modeling these novel devices require evaluation and verification, and experimental measurement of the structure's response comprises the core of the verification process.

Both out-of- plane and in-plane displacement components must be measured over a large portion of the structure's surface to provide sufficient data for verification. Such measurements must be made using noncontacting techniques because the installation of contacting sensors would dramatically affect the dynamic response of the surface under observation. Measurement of the in-plane component of surface displacement is the more challenging of the two measurements and requires either a nonreflecting surface or a pattern that was fabricated on the surface either by deposition or etching.

Before the experimental work described herein, a survey of established in-plane measurement approaches was performed to determine which was most appropriate for this particular application. Geometric moiré, moiré interferometry, laser speckle tracking, electronic laser speckle interferometry, and optical feature tracking with digital image processing were identified as the most likely candidates. Each of these techniques requires different surface geometries, and all possess different measurement ranges and sensitivities. A summary of the capabilities of each method is contained in Table 1.

Parts V and VII of Cloud [1] provide a good overview of the moiré and speckle techniques summarized in Table 1. Both of these general approaches for tracking in-plane surface motion have been in common usage for many years, as indicated by the diverse array of applications in which they have been used [2–9].

Because the goal of this research was to accomplish dynamic tracking of all in-plane motion components simultaneously, both of the moiré methods were eliminated from consideration, due to the limitations listed in the dynamic/real-time tracking row of Table 1. At the time this research was commenced, the resolution of the electronic speckle pattern interferometry method was limited, due to its dependence on video. Laser speckle tracking, although particularly attractive because it does not require a special surface preparation, was eliminated from consideration because of its limited measurement range [1]. Examples of pattern tracking found in the literature have shown the feasibility of using computational image analysis to track the motion of surface features through sequences of successive images.‡‡ The in-plane tracking range of this method is limited only by the field of view of the camera(s) used, and the measurement resolution is generally related to the physical distance on the tracked object corresponding to a single camera pixel. Because of its flexibility and relative simplicity, optical pattern tracking was chosen as the method to be used for the experimental portion of this work.

Some groundwork for the monitoring of in-plane motion components via pattern tracking had already been accomplished

Presented as Paper 1805 at the 7th AIAA Gossamer Spacecraft Forum, Newport, RI, 1–5 May 2006; received 1 June 2006; revision received 1 June 2007; accepted for publication 12 August 2007.

*Assistant Professor, Department of Engineering Science, One Trinity Place. Member AIAA.
†Ph.D. Student; currently Assistant Professor, U.S. Air Force Institute of Technology. Member AIAA.
‡Donald and Gertrude Lester Professor of Mechanical Engineering, 279 Ralph G. Anderson Building. Member AIAA.
§Graduate Research Assistant, Department of Electrical and Computer Engineering.
¶Associate Professor, Department of Electrical and Computer Engineering, 697 F. Paul Anderson Tower.

**Data available online at http://antwrp.gsfc.nasa.gov/apod/ap040821.html [retrieved 8 October 2007].
††Data available online at http://ngst.gsfc.nasa.gov [retrieved 1 June 2006].
‡‡Data available online at http://www.grc.nasa.gov/Other_Groups/RT1998/6000/6729klimek.html [retrieved 31 May 2007].

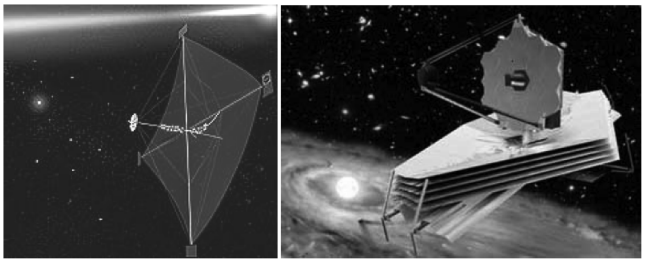

Fig. 1 Concept designs for solar sails and the planned James Webb Space Telescope (courtesy of NASA Goddard Space Flight Center).

before this work commenced. For instance, the problem of fabricating patterns into the surface of a metallized thin film was studied by Thota [10] and Thota et al. [11]. In this work, small test articles were prepared by mounting sheets of metallized thin film to copper retaining rings and then etching a variety of candidate patterns into the surface of each test article using a krypton fluoride (KrF) excimer laser. After preliminary evaluation, a pattern consisting of a set of filled circles was selected as the best candidate for pattern tracking. *Videogrammetry* [12], a noncontact measurement technique dating from the 1970s, is a multicamera optical pattern tracking approach that has been used (under a variety of names) to track the motion of complex bodies, especially in the automotive and medical fields [13–15]. Videogrammetry is based on *photogrammetry*, a static measurement technique that uses the process of triangulation to reconstruct the three-dimensional surface shape of an object from a series of two-dimensional images simultaneously taken from various vantage points [16]. In videogrammetry, multiple sets of images (frames) are taken sequentially at a high rate, allowing the three-dimensional position of a target array to be tracked as a function of time. Assuming a sufficiently dense target array was chosen, this technique can potentially enable an object's overall surface motion to be reconstructed. This paper reviews the fabrication techniques used to develop the patterned test articles, as well as the process of measuring and calculating the surface displacement components of a moving and deforming test article using videogrammetry. In addition, an estimate of the surface measurement resolution is discussed.

II. Test-Article Design and Fabrication

Thin-film metallized test articles similar to the one shown in Fig. 2 were prepared using a laser ablation technique, in which the pattern array (a series of 1.00-mm-diam circular dots on a 5.0-mm pitch) was etched into the surface of metallized thin film using a KrF excimer laser system. The laser settings chosen to produce the pattern depended principally on the thickness and composition of the metallization and were determined based on results obtained by Thota [10] and Thota et al. [11] in a prior study. Primary factors affecting pattern quality on the surface of the test article included specification of the 1) energy of the laser pulse, 2) aperture size through which the beam passes, 3) beam focus, 4) pressure inside the test sample chamber, and 5) laser pulse spacing. Because the aluminum-coated films used here were similar to those studied by Thota [10], his set of laser parameters (Table 2) were chosen to produce the pattern shown in Fig. 2.

Table 2 Optimized laser parameters for pattern fabrication (from Thota [10])

Laser energy	150 mJ/pulse
Beam splitter	60%
Angle of variable attenuator	30 deg
Pulse spacing	30.48 μm
Vacuum chamber pressure	2×10^{-2} torr

Before etching, the test articles were assembled by taking 12.7-μm-thick (0.5-mil-thick) polyester films coated on one side with a 0.2-μm aluminum layer (in sheet form) and using silicone adhesive to attach each one to 2-mm-thick copper rings with a 76.45-mm (3.01-in.) inner diameter and a 117.7-mm (4.64-in.) outer diameter. These particular dimensions represented the largest sample size that could fit onto the stage of the excimer laser machining equipment in the University of Kentucky Laser Processing Laboratory. Finite element studies that were performed verified that removing up to 5% of the total metallization area from the surface of the film had a negligible effect on the modal response of the test structure [10,11].

III. Experimental Procedure

To verify the ability of the videogrammetry technique to simultaneously track the full-field in-plane and out-of-plane surface motion of a moving and/or deforming structure, the patterned test article was installed in an aluminum holder. An L-shaped aluminum beam (3.175×25.4 mm rectangular cross section) was mounted to two of the threaded holes provided on the rear of the aluminum holder (Fig. 3). That assembly was, in turn, attached to the top surface of a long-stroke electrodynamic shaker by positioning the slotted section of the L-shaped beam (shown) directly above a row of threaded holes provided on the top surface of the shaker. The beam was clamped to the shaker (Fig. 4) using two threaded bolts and washers.

A 1-Hz sine wave was supplied by a function generator and linear amplifier to the shaker, which applied a vertical excitation to the test article that was primarily in the in-plane z direction. A sequence of

Table 1 Summary of capabilities of in-plane sensing methods

	Geometric moiré	Moiré interferometry	Pattern tracking	Laser speckle tracking	Electronic speckle pattern interferometry
Full field or point	Full	Full	Multiple points	Multiple points	Full
Resolution (order of magnitude)	10 μm (120 lines/mm)	1 μm (1200 lines/mm)	10 μm (video: 1-cm linear distance on test object; 1000 pixels imaging that dimension)	1 μm ($\sim$1 optical wavelength)	20 μm (limited by video)
Surface preparation	Grid or grating	Grid or grating	None if a suitable pattern already exists on the surface	None	None, as long as the surface totally diffuses incoming light
Light source	Any	Coherent	Any	Coherent	Coherent
In-plane displacement components	All in simultaneous measurement	All, simultaneous measurement is not possible	All	All	All
Dynamic/real-time tracking	Difficult due to low fringe contrast	One component at a time	Yes	Yes	Yes

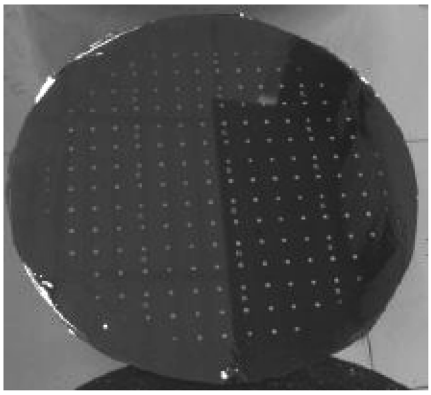

Fig. 2 Image of the patterned thin-film mirror sample containing an array of 1.00-mm-diam circles on a 5.0-mm pitch (from Ma [18]).

Fig. 3 L-shaped beam used to mount the film holder to the modal shaker. Note the arrows demarcating the clamping locations on the lower portion of the beam. The scale shown on the left side of the ruler corresponds to inches.

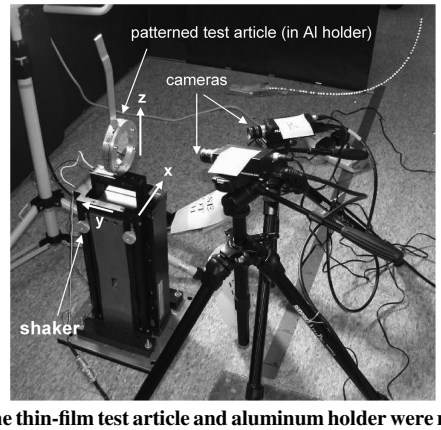

Fig. 4 The thin-film test article and aluminum holder were mounted on an electrodynamic shaker using the slotted aluminum beam. The two videogrammetry cameras are shown to the right of the shaker. Coordinate directions (but not the origin) are indicated, with the shaker stroke direction corresponding to the *z* direction.

synchronized images used to track the test-article motion and surface deformation was taken using the two pictured Pulnix TM-6710CL synchronized progressive scan cameras, each of which was capable of producing images of 650 (wide) by 450 (high) pixels at a theoretical maximum rate of 120 frames per second. The two cameras were oriented so that their respective image planes were about 90 deg apart and were positioned so that the test article filled the field of view of each. The thin-film test article was illuminated in

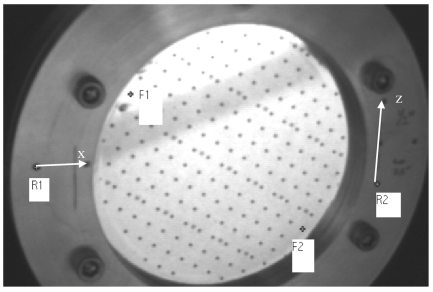

Fig. 5 Cropped view of one of the test images used to reconstruct the surface geometry of the thin-film material. The distance between targets R1 and R2 (each demarcated by a + above their respective labels) on the Al film holder was expected to remain constant, whereas the (in-plane) distance between targets F1 and F2 on the thin-film material (each demarcated by a bold +) was expected to change due to modal response. Note the *x* and *z* coordinate directions; *y* is oriented into the thickness of the film holder and is perpendicular to both *x* and *z*.

an indirect manner using bright halogen lights distributed around the perimeter of the work space. Each light was directed away from the test article, toward white draping material that was used to surround the experimental work space. This brightly illuminated material maximized the visibility of the etched targets by ensuring that the image reflected by the surface of the test article would be bright and uniform, allowing good contrast between each target and the surrounding surface. Without the use of uniform draping around the perimeter of the test article, the thin-film surface would reflect objects, including light sources, in the same way that a mirror does; such reflected images would create a very visually complex *surface texture* that would affect the contrast between each target and the background. An example of this effect is present in the targeted membrane shown in Fig. 2. Furthermore, using lights to directly illuminate the test article would create an even more difficult situation, resulting in glares and glints on the surface that would in all likelihood completely obscure the visibility of the etched targets.

The experimental images were captured by a customized PC (with 4-GB RAM, an Intel Xeon processor, and a 64-bit PCIX bus operating at 133 MHz) containing a DVR Express high-speed video capture board. The individual images used for reconstruction were obtained using Video Savant 4.0 Frame Grabber software. In this particular experiment, the camera imaging speed was 75 Hz, and all points visible in Fig. 5 were recorded for 4 s, and hence were available for further analysis. However, in this study, only the motion of four points (two points on the outer circumference of the aluminum fixture used to hold the thin-film mirror and two of the circular points etched into the thin-film itself) was explored in detail.

Although the distance between the two points on the aluminum film holder was expected to remain constant as a function of time (because it was moving in a primarily rigid-body mode), the distance between the two points tracked on the test article was expected to vary, on account of the modal response in the thin film caused by the sinusoidal input from the shaker. Variation in the distance calculated between the two points on the (virtually rigid) aluminum test fixture as a function of frame number (which is directly related to elapsed time) therefore can be used to estimate the in-plane tracking resolution of the system. This approach is similar to one used by Mesqui et al. [15] to determine system tracking resolution. The videogrammetric processing employed for this series of measurements was performed by the PhotoModeler Pro 5.0 video module. Calibration of the video cameras was accomplished using the automated procedure provided by the videogrammetry software, with the calibration target image (provided with the software) sized to fill the cameras' fields of view.

IV. Results

A. Three-Dimensional Displacement Tracking of Individual Points

The basic ability of the videogrammetry system to track in- and out-of-plane motion was evaluated by simultaneously tracking two

target points on the flexible thin-film test article (F1 and F2 in Fig. 5) and two target points on the aluminum film holder (R1 and R2 at the tail end of each arrow in Fig. 5) that served as benchmarks for comparison. The target points on the film were formed using the laser ablation technique discussed in Sec. II, and the points on the sample holder were created with a black 0.5-mm permanent-ink marker. The six points on the aluminum film holder were expected to remain fixed relative to each other, which allowed them to be used to benchmark the motion of the film. The assumption that the aluminum film holder would primarily respond in a rigid-body mode was made based on its high stiffness, coupled with the very low (1-Hz) excitation frequency and displacement amplitude. The six fixed points placed on the film holder were also used for scaling purposes and to establish the xyz coordinate directions within the photogrammetry software.

As mentioned previously, the film holder was attached to a 3.175×25.4 mm (0.125×1.00 in.) aluminum beam, the end of which was securely fastened to the shaker. This method of mounting the film holder was expected to provide a virtually rigid connection between the vertical axis of the shaker and the test article in the in-plane x and z directions. However, because the film holder was, in effect, cantilevered to the aluminum beam (Fig. 3), it was expected that out-of-plane y vibration modes would likely be generated due to modal coupling.

Because they were located on the aluminum film holder, the z component of motion of points R1 and R2 was expected to be quite similar to the input motion provided by the shaker (vertical-motion amplitude approximately equal to 1.5 mm at $f = 1$ Hz). This, in fact, was the case (Fig. 6), because the measured z coordinates of points R1 and R2 seemed to have both the expected amplitude and frequency and only differed from each other by the constant offset shown in the plot. This constant z offset is likely related to the physical locations of points R1 and R2 on the film holder.

Inspection of the x and y components of motion of points R1 and R2 shows that they, too, are nonzero, which means that other in- and out-of-plane motion components have presumably been induced in the film holder. Figures 7 and 8 indicate that in addition to the dominant z motion caused by the shaker input, a small pure translational component in the x direction was applied to the film holder. The determination that this component was purely translational was based on a comparison of both the amplitude and phase of the x component of displacement of the points, which were both quite similar to each other. If there had been a rotational component of motion present, the amplitudes of the plots shown in Figs. 7 and 8 would have differed from each other. For both points, the x direction displacement amplitude was consistently about 5% of that measured in the z direction (Fig. 6). It is most likely that this small in-plane translation component in the x direction was caused by a slight misalignment between the vertical array of points (used to set the z direction within the PhotoModeler software), shown on the right side of the film holder in Fig. 5, and the true vertical axis of the shaker.

Figures 9 and 10 show that the out-of-plane y motion components of points R1 and R2 differed from each other in both amplitude and phase and that they contained frequency content that was

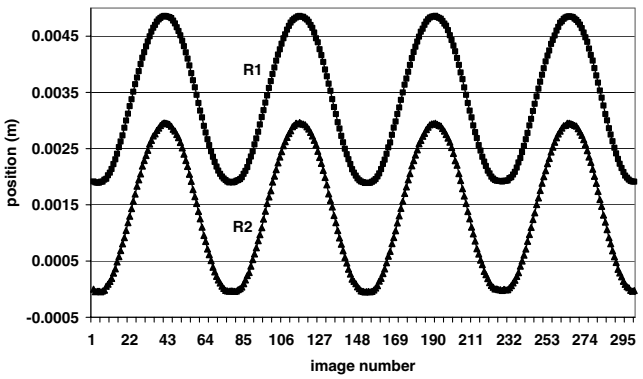

Fig. 6 The z component of the motion of points R1 and R2 on the aluminum film holder was primarily dependent upon the in-plane excitation motion provided by the shaker (z-motion amplitude approximately equal to 1.5 mm and $f = 1$ Hz). The offset between the plotted curves is approximately equal to the physical vertical offset between the physical positions of R1 and R2 on the aluminum sample holder (Fig. 5). The images used to calculate the position data were obtained at 75 Hz, and so the data shown here (and those in all subsequent figures), obtained using 300 sets of images, represent 4 s of motion. The total distance range shown on this plot is 5.5 mm.

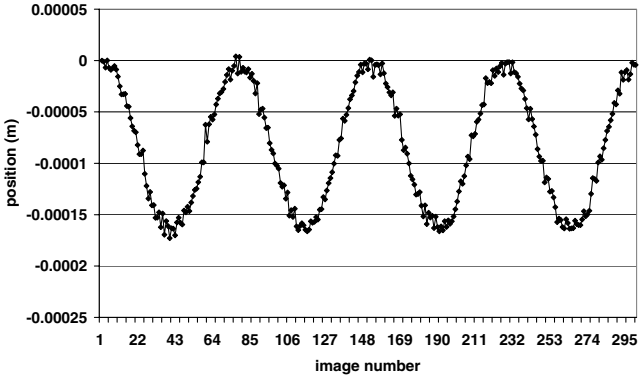

Fig. 7 Although the primary excitation motion was in-plane along the z direction, point R1 on the film holder also exhibited an in-plane x component of motion, for which the amplitude was less than 5% of the z component (Fig. 6). This discrepancy was most likely due to a misalignment between the z axis (as set using the PhotoModeler software) and the true vertical axis of the shaker. The total distance range shown on this plot is 0.3 mm.

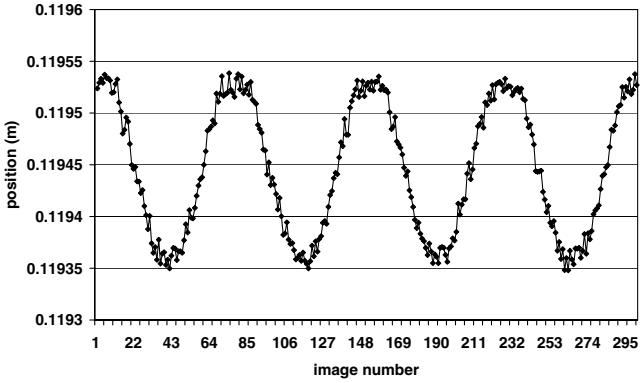

Fig. 8 The amplitude and phase of the in-plane x component of motion of point R2 on the sample holder was virtually identical to that of point R1, shown in Fig. 7. The total distance range shown on this plot is 0.3 mm.

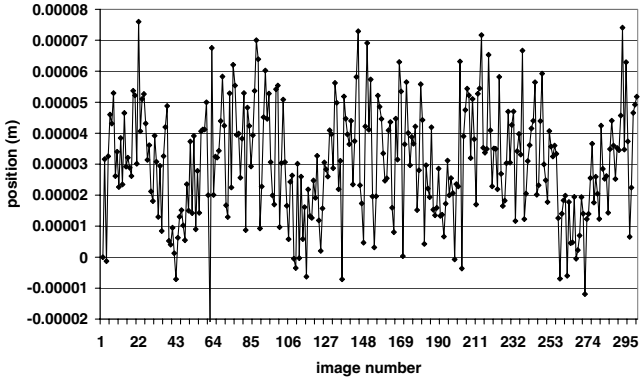

Fig. 9 The out-of-plane y motion component of point R1 indicates some dependence on the 1-Hz shaker input, but also shows a great deal of higher-frequency content. The total distance range shown on this plot is 0.1 mm.

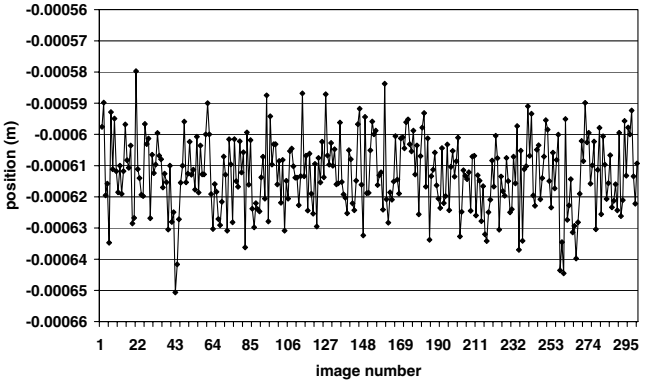

Fig. 10 In the out-of-plane *y* direction, point R2 shows an overall smaller range of motion than point R1, as well as virtually no dependence on the 1-Hz shaker input. The total distance range shown on this plot is 0.1 mm.

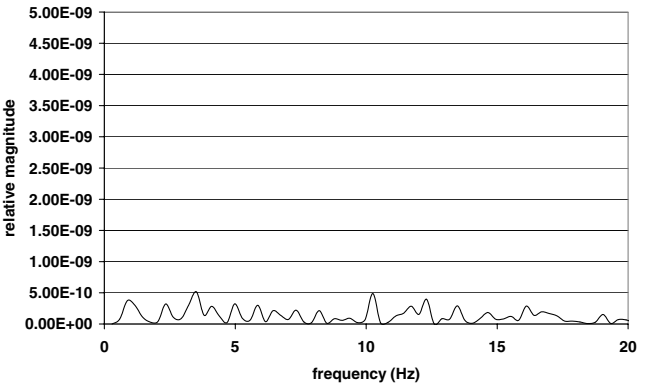

Fig. 12 Frequency power spectrum of the *y* component of motion of point R2 (on the aluminum film holder). The low magnitude of the spectrum and lack of any dominant frequency component imply that there was little, if any, frequency-dependent component of motion in the *y* direction at this particular location.

substantially different from that provided by the shaker input. As stated previously, this out-of-plane motion was likely caused by the compliance of the thin cantilever beam used to connect the film holder to the shaker, as well as the geometry of the mounting scheme used. Because the locations of points R1 and R2 were not exactly symmetric with respect to the attachment point of the aluminum film holder on the beam, the modal coupling at each location was likely dissimilar. After producing a frequency power spectrum for both displacement profiles shown in Figs. 9 and 10, a prominent low-frequency response (between 1 and 3 Hz) in the *y* direction was found to exist at point R1 on the aluminum holder (Fig. 11). However, no similar frequency-dependent out-of-plane motion was observed at point R2 (Fig. 12).

If the film showed a purely rigid response, the displacement components of the tracked points on the film (F1 and F2) would likely only differ from those on the holder (R1 and R2) by the constant offsets related to point location geometry shown in Fig. 5. However, the compliance of the thin-film sample made a purely rigid response quite unlikely, and the presence of in- and out-of-plane motion components induced by the motion of the shaker is readily observed even in the time domain. Although the *z* components of motion of points F1 and F2 on the film (Fig. 13) strongly resemble the *z* components of motion of points R1 and R2 on the aluminum holder (Fig. 6) to within a constant offset value, there are major differences apparent between the in-plane *x* components of motion on the aluminum holder (Figs. 7 and 8) and on the film (Fig. 14). Although the 1-Hz sinusoidal component provided by the shaker excitation is readily apparent in both the *x* component responses of the aluminum holder and the film, points F1 and F2 on the thin film (Fig. 14) show more superimposed high-frequency content.

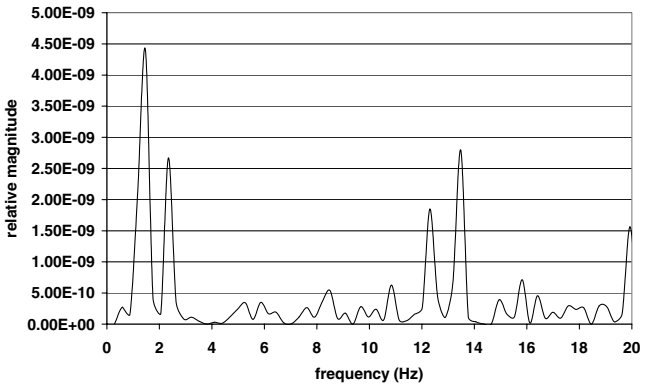

Fig. 11 Frequency power spectrum of the *y* component of motion of point R1 (on the aluminum film holder). Note the relatively strong frequency peak centered around 1 Hz. A digital imaging speed of 75 Hz limited the Nyquist frequency to 37.5 Hz for this and all subsequent frequency power spectrum plots.

The out-of-plane *y* motion component of points F1 and F2 differ from both each other (Fig. 15) and from each of the points tracked on the aluminum holder (Figs. 9 and 10). Most prominently, at both tracked locations on the film, the amplitude of *y* component motion is often larger than is the case at either point on the aluminum holder. This could be caused by lack of tautness in the thin-film test article or

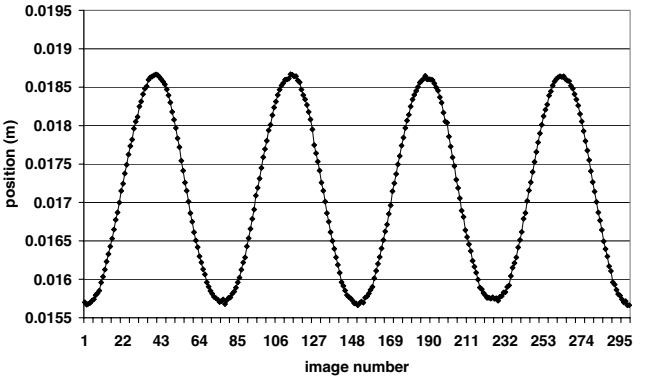

a) Point F1

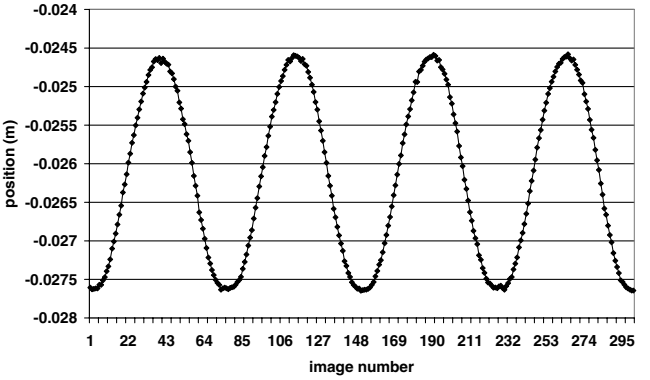

b) Point F2

Fig. 13 The *z* component of the motion of points F1 and F2 on the thin film was primarily dependent upon the excitation motion provided by the shaker (*z*-motion amplitude approximately equal to 1.5 mm and $f = 1$ Hz). The offset between the two curves (plotted using the same vertical scale) is approximately equal to the physical vertical offset between the positions of F1 and F2 on the aluminum film holder (Fig. 5). However, close examination of the plots shows some deviation from a pure translational (sinusoidal) response, as evidenced by the slight "jaggedness" that is most apparent at the vertical extrema. The total distance range shown on these plots is 4.0 mm.

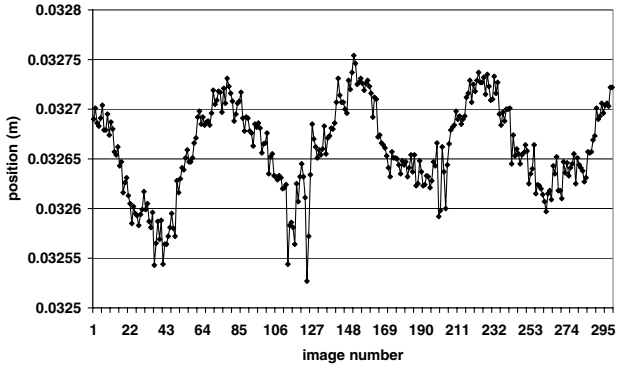

a) Point F1

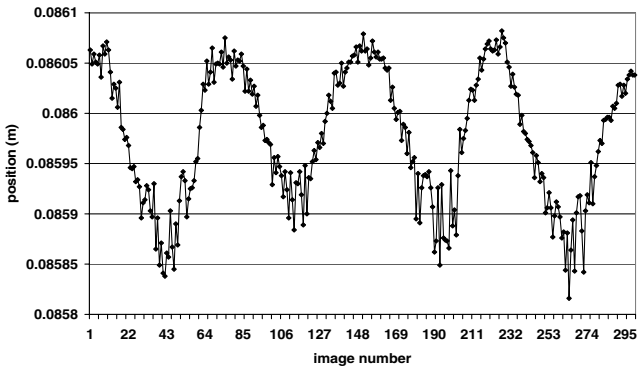

b) Point F2

Fig. 14 The *x* component of motion at points F1 and F2 on the thin film. As before, the 1-Hz sinusoidal contribution to the motion, likely caused by a slight misalignment between the direction of the *z* axis (as defined within the photogrammetry software) and the true vertical axis of the shaker, is readily apparent. However, the *x* component of motion of points F1 and F2 has significantly more high-frequency content than that of points R1 and R2 on the aluminum film holder, shown in Figs. 7 and 8. Note that the total distance range shown on these plots is 0.3 mm.

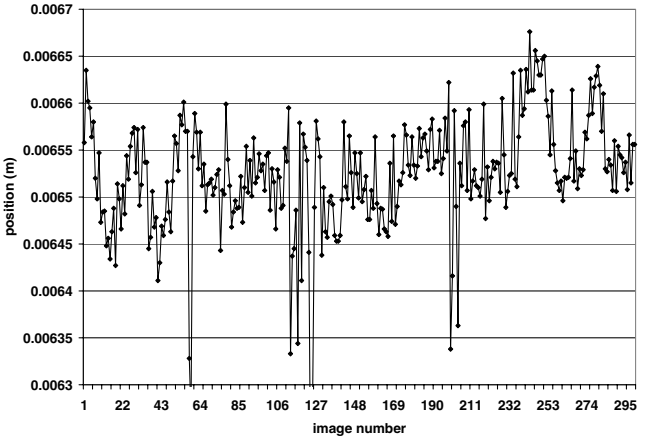

a) Point F1

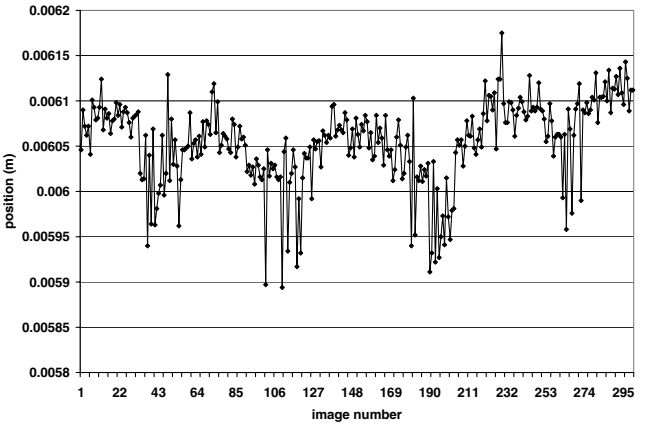

b) Point F2

Fig. 15 The out-of-plane *y* component of motion of points F1 and (especially) F2 in the thin film both seemed to depend on the 1-Hz in-plane excitation provided by the shaker. Note that the total distance range shown on these plots is 0.4 mm.

by cyclical aerodynamic loading of the test article due to simple air resistance. Figure 16 shows the frequency content of the y component of motion at both locations on the film. The out-of-plane motion of both F1 and F2 contains significant frequency content near 1 Hz, the in-plane excitation frequency.

B. Measurement of Experimental In-plane Displacement Resolution

The term *in-plane displacement* can be interpreted in a number of ways. Here, we have adhered to a definition that sets the in-plane displacement of a deforming surface as the change in straight-line distance between the centroids of two target points on the surface. In this particular experiment, the change in line length between points F1 and F2 (on the film) is compared with the change in line length between points R1 and R2 (on the film holder). Because the aluminum sample holder was translated in rigid-body motion (z-motion amplitude approximately equal to 1.5 mm and $f = 1$ Hz) in the in-plane direction, no physical change in the distance between points R1 and R2 was expected. Hence, any change in distance between the centroids of points R1 and R2 measured using the videogrammetry system could be construed as a direct measurement of the system's minimum-resolvable displacement resolution, or noise floor. In contrast, because the thin film has a low stiffness, any measured change in distance between the centroids of points F1 and F2 (greater than the inherent system resolution) can be assumed to indicate an in-plane film deformation. The cause of this deformation was likely an out-of-plane modal response induced by the in-plane motion of the shaker. The distance between each set of points was calculated using the position information obtained in the previous section, by computing the magnitude of the vector connecting the two points:

$$L = \sqrt{(x_2 - x_1)^2 + (y_2 - y_1)^2 + (z_2 - z_1)^2} \tag{1}$$

where L is the length of the line connecting the centroids of the two points on either the film or aluminum holder, and x_1, y_1, z_1, x_2, y_2, and z_2 are the measured coordinates of each point.

After analyzing 4 s of videogrammetry data, which, as stated previously, corresponds to 300 sets of images, L_r, the mean value of the distance between points R1 and R2 on the aluminum sample holder, was computed to be 0.11954 m and $\sigma = 10.97$ μm, and L_f, the mean value of the distance between points F1 and F2 on the film, was computed to be 0.06867 m and $\sigma = 56.6$ μm. The videogrammetrically measured distances used to calculated the respective means are both plotted in Fig. 17 as a function of image number. Clearly, the variation in distance between points F1 and F2, as indicated by both the harmonic component of the time-domain plot and the calculated value of the measurement standard deviation σ, is an indication of a modally induced in-plane deformation of the film. In contrast, the standard deviation σ calculated based on the variation of the measured distance between points R1 and R2 on the aluminum holder was much smaller, and the distance variation between R1 and R2 over the measurement period showed a much weaker harmonic dependence. Because the *physical* distance between the centroids of points R1 and R2 was expected to remain constant due to the high stiffness of the aluminum, as well as to the low amplitude and frequency of the excitation motion, the calculated value of $\sigma = 10.97$ μm due to the scatter in the data is likely an indication of the system's noise floor or best measurement resolution possible using this particular combination of equipment (i.e., cameras and videogrammetry software) and camera placement.

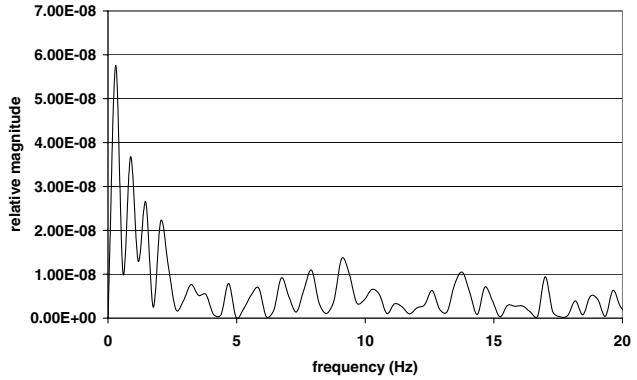

a) Point F1

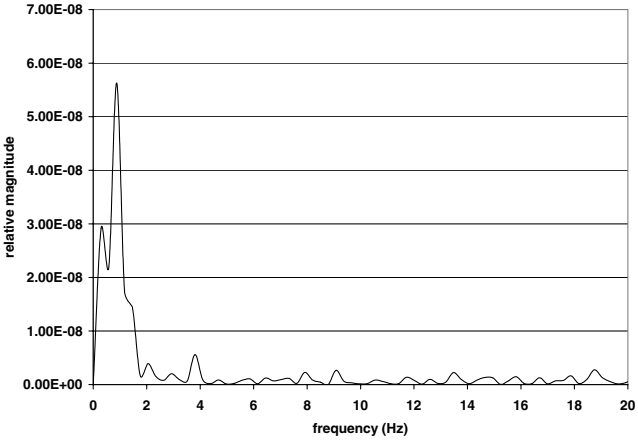

b) Point F2

Fig. 16 Frequency power spectrum of the *y* component of motion of points F1 and F2 on the thin film. Although both plots clearly show low-frequency content centered on 1 Hz, the motion of point F2 seems to be more closely coupled to the in-plane 1-Hz excitation provided by the shaker. Note that both power spectra are shown using the same vertical scale.

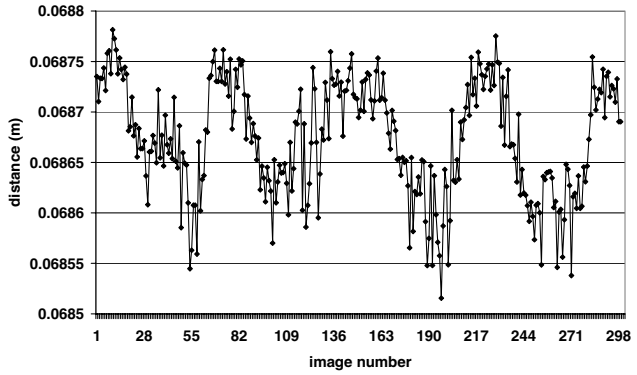

a) Points F1 and F2 (on film)

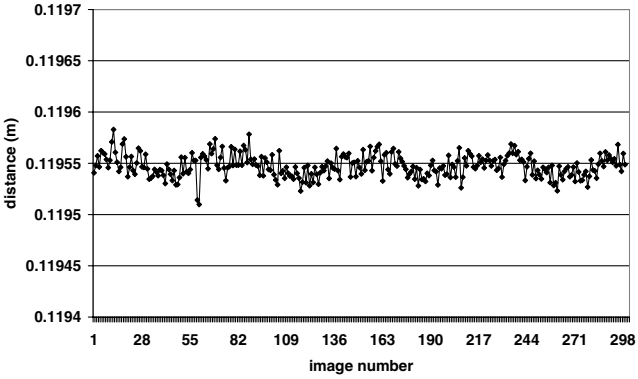

b) Points R1 and R2 (on holder)

Fig. 17 The videogrammetrically measured distance between the two points tracked on the aluminum fixture (bottom) clearly remains virtually constant, whereas the videogrammetrically measured distance between the two points tracked on the film varies significantly (top) when the sample was subjected to the 1-Hz, 1.5-mm, in-plane *z* excitation provided by the shaker. Note that the total distance range represented on the vertical axes of both plots is the same (0.3 mm).

V. Discussion

A. Test-Article Fabrication

The excimer laser patterning of the thin-film test articles was easily achieved with a single low-energy pulse per spot, over the limited area shown. However, the maximum area that can be patterned using the laser ablation technique is limited by certain physical constraints imposed by the patterning equipment. For instance, the excimer laser machining system used for this work (located in the Laser Processing Laboratory at the University of Kentucky) has a motion stage with 101.6×203.2 mm (4×8 in.) travel, stepper motor control, and a vacuum chamber for processing in pressure-controlled atmospheres. The test articles were processed in air with a 248-nm wavelength (KrF) fixed-position laser beam and was moved by the stage to enable the laser beam to impinge on all areas of the surface. However, even removal of the vacuum chamber and construction of a suitable mounting fixture would not allow complete area patterning of the 355.6-mm-diam (14-in.-diam) samples originally obtained for this study. Although it may be possible to pattern a portion of the sample surface and then remount the sample to allow an adjacent portion of the surface to be patterned, alignment of the overall pattern would be limited to the mounting hardware reliability. Although a moving stage could be used to reposition the film relative to the laser beam, larger samples patterned in this way would tend to respond modally during the patterning process, with high-amplitude, low-frequency, out-of-plane motion induced as the stage moved. Because the excimer laser spot is imaged onto the plane of the film, such high-amplitude oscillations would likely move the film in and out of the image plane. This would likely reduce the sharpness of the spot delivered to the metallization surface, adversely affecting the quality of the final pattern. This effect could possibly be partially mitigated by varying the value of the pressure under the film within the patterning chamber (assuming a suitably sized pressure-controlled chamber could be used).

Commercial laser machining systems have moving stages such as that described in the previous paragraph, to which stock material is clamped. Another approach taken by certain other commercial systems allows the sample to be held stationary while the laser head is moved over the material to create a pattern. Either one of these system types would be capable of completely patterning a 355.6-mm-diam metallized film. Larger area films viewed at greater distances may require larger pattern features (depending on the camera resolution) to accurately measure displacements to the desired precision. If the required feature size exceeds the laser beam-spot dimensions, then the laser can be rastered to remove the metal film over a specified region, which would decrease the processing rate when compared with that obtained using the single-pulse nonrastered patterning technique used in this study.

It is also possible that other laser types operating at wavelengths other than that used here could be used to remove the metallization layer without damaging the underlying polymer. Before using another type of laser to create such patterns, a parametric study similar to that performed in this work will be required to determine the appropriate energy settings, spot size control, and atmosphere. Because most commercial systems run continuous-wave beams at high energy for cutting metal materials, the fragile nature of the foils and thin metal layer would pose a significant challenge. However, pulsed laser systems, such as frequency-doubled or frequency-tripled Nd:YAG are more likely to be successful at removing the metal without damaging the underlying polymer. Such pulsed beams

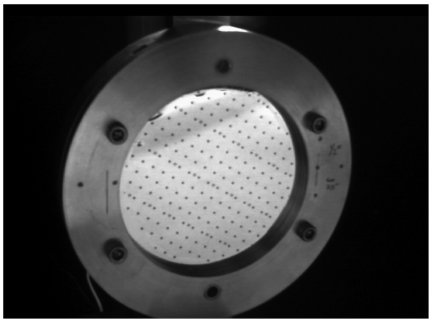

Fig. 18 The height of this test image (used in the videogrammetric reconstruction) is about 125 mm.

would be able to generate the desired spot patterns more easily than a continuous-wave laser. Excimer laser machine shops are also available that contain equipment that possesses more sophisticated motion control systems than that used here. Such systems would be capable of replicating the ablation parameters used to process the thin films described herein and would be able to reproduce the desired pattern over a larger surface area.

B. Videogrammetric Measurement

Regarding the analysis of the motion of the test-article holder and the film, the following must be noted. First, the motion of only two points on the thin-film test article and two points on the aluminum frame was fully analyzed here. However, the methods described in this study could easily be extended to sufficient numbers of additional points on the surface of the test article, to obtain a full-field description of its surface motion. Second, some of the results reported in Sec. IV (Results) were attributed to "induced modal response"; however, neither numerical nor analytical predictions of the modal behavior of the test article and aluminum holder were presented for comparison. Such predictions were omitted because the focus of this paper was on the measurement technique and test-article processing, not the determination of the modal response of the test article and aluminum film holder.

Finally, it was stated previously that the scatter in the measured distance between points R1 and R2 on the aluminum holder could be taken as an estimate of measurement resolution. It turns out that this value, $\sigma = 10.97\ \mu$m, is somewhat smaller (but still of similar magnitude) than that obtained by estimating resolution based on the number of pixels on the imaging element, the physical size of the object under study within the camera's field of view, and the technique used to identify the exact locations of targets within images. Considering the ratio of image height in Fig. 18 (about 125 mm) to the number of pixels along the imaging sensor in the same direction (480), each pixel in the images used in this study represents a physical distance of about 0.26 mm on the test article. A study by Pappa et al. [17] determined that measurement resolution using consumer-grade digital cameras with the software package (PhotoModeler) employed here often exceeds one-tenth of a pixel. The conservative estimate of system resolution calculated using Pappa's approach (26 μm) is similar in magnitude to the value (10.97 μm) reported previously using the standard deviation of the measurement data as the benchmark value for the noise floor, or minimum-resolvable displacement. Given that the Pappa et al. method provides a conservative indirect estimate of minimum resolution, it is not surprising that the direct measurement of experimental scatter used herein provides better results.

VI. Conclusions

In this study, an electrodynamic shaker was used to provide an in-plane harmonic excitation to a thin-film membrane mounted in an aluminum test fixture. Because of the low frequency (1 Hz) and low amplitude (1.5 mm) of the excitation, it was expected that the aluminum test fixture would exhibit only rigid-body motion, whereas the compliant thin film was expected to exhibit both in- and out-of-plane deformation modes. Using a two-camera videogrammetry setup that imaged the test article at a frequency of 75 Hz, the x, y, and z motion components of two points on the thin film (F1 and F2) and two points on the aluminum holder (R1 and R2) were simultaneously tracked for 4 s. The points of interest were located in each of the 600 images collected (300 per camera), and their position relative to a fixed coordinate system was identified via a triangulation calculation performed by the videogrammetry software.

It was found that the z component of motion (in-plane) of all the tracked points was virtually identical in both amplitude and frequency to the excitation provided by the shaker. A 1-Hz in-plane component of motion in the x direction, for which the amplitude was about 5% of that found for the z component, was also found for each of the points tracked. It was assumed that this unexpected motion component stemmed from a misalignment between the z direction, as defined within the videogrammetry package, and the vertical axis of the shaker. Only one of the points tracked on the aluminum holder (R1) seemed to exhibit an out-of-plane y component of motion that was induced by the shaker excitation. The harmonic content of the motion, for which the amplitude did not exceed 0.05 mm, was confirmed by the frequency power spectrum shown in Fig. 11. It is also clear (based on the frequency power spectrum shown in Fig. 12) that the out-of-plane motion component of point R2 was not directly caused by the in-plane harmonic excitation, because no prominent 1-Hz peak was discerned. The reasons for this difference are unclear. On the film, both points F1 and F2 exhibited out-of-plane displacements that clearly originated from the 1-Hz in-plane excitation, as confirmed by the frequency power spectra depicted in Fig. 16.

To determine whether in-plane deformations were generated within the film, the distances between the two points on the film, as well as between the two points on the aluminum holder, were tracked over the 4-s sampling interval. Because the aluminum film holder was excited in-plane, in a rigid-body mode, it was expected to move without any deformation, and the distance between points R1 and R2 was expected to remain virtually constant despite the shaker input. This was, in fact, the case, and the standard deviation of these measured distances, $\sigma = 10.97\ \mu$m, was used as an estimate of the resolution of the system's in-plane tracking ability. This resolution exceeded the value for measurement resolution (26 μm) approximated using Pappa's method [17], which is based on pixel density and field of view. Because the variation in distance between points F1 and F2 was much larger during the course of the measurement, it was assumed that this, in fact, indicated the presence of in-plane deformation within the film.

Acknowledgments

The work described in this paper was funded in part by the Kentucky Science and Engineering Foundation, under contract KSEF-148-502-02-32. The first author is grateful to Phanikrishna Thota for his useful comments on the draft.

References

[1] Cloud, Gary, *Optical Methods of Engineering Analysis*, Cambridge Univ. Press, New York, 1998.

[2] Post, D., "Moire Interferometry: Advances and Applications," *Experimental Mechanics*, Nov. 1991, pp. 276–280. doi:10.1007/BF02326072

[3] Aebischer, H. A., and Waldner, S., "A Simple and Effective Method for Filtering Speckle- Interferometric Phase Fringe Patterns," *Optics Communications*, Vol. 162, Nos. 4–6, 1999, pp. 205–210. doi:10.1016/S0030-4018(99)00116-9

[4] Sarrafzadeh-Khoee, A., and Duke, J. C., Jr., "Small In-Plane/Out-Of-Plane Ultrasonic Displacement Measurement Using Laser-Speckle Interferometry," *Experimental Techniques*, Oct. 1986, pp. 18–21.

[5] Sjodahl, M., "Electronic Speckle Photography: Measurement of In-Plane Strain Fields Through the Use of Defocused Laser Speckle," *Applied Optics*, Vol. 34, No. 25, Sept. 1995, pp. 5799–5808.

[6] Singh, M., and Ramachandran, G., "Reconstruction of Sequential Cardiac In-Plane Displacement Patterns on the Chest Wall by Laser Speckle Interferometry," *IEEE Transactions on Biomedical Engineering*, Vol. 38, No. 5, May 1991, pp. 483–489. doi:10.1109/10.81568

[7] Sirohi, R. S., Burke, J., Helmers, H., and Hinsch, K. D., "Spatial Phase Shifting for Pure In-Plane Displacement and Displacement-Derivative Measurements in Electronic Speckle Pattern Interferometry (ESPI)," *Applied Optics*, Vol. 36, No. 23, Aug 1997, pp. 5787–5791.

[8] Tong, J., Zhang, D.-S., Li, H.-Q., and Li, L.-N., "Study on In-Plane Displacement Measurement Under Impact Loading Using Digital Speckle Pattern Interferometry," *Optical Engineering*, Vol. 35, No. 4, Apr. 1996, pp. 1080–1083. doi:10.1117/1.600787

[9] Waldner, S., and Kress, G., "Nondestructive Testing of Composite Materials with Electronic Speckle Pattern Interferometry and Shearography," *Trends in Optical Non-Destructive Testing and Inspection*, edited by Pramod Rastogi and Daniele Inaudi, Elsevier, Oxford, 2000, pp. 257–271.

[10] Thota, P., "Pattern Evaluation for In-Plane Displacement of Thin Films," M.S. Thesis, Department of Mechanical Engineering, Univ. of Kentucky, Lexington, KY, Aug. 2003.

[11] Thota, P., Leifer, J., Smith, S. W., and Lumpp, J. K., "Pattern Evaluation for In-Plane Displacement of Thin Films," *Experimental Mechanics*, Vol. 45, No. 1, Feb. 2005, pp. 18–26. doi:10.1007/BF02428986

[12] Black, J. T., and Pappa, R. S., "Videogrammetry Using Projected Circular Targets: Proof-of-Concept Test," NASA TM-2003-212148, Feb. 2003.

[13] Kay, I. W., and Zobel, E. C., "Simplified Three-Dimensional Photogrammetric Analysis of Moving Bodies," Automotive Engineering Congress, Society of Automotive Engineers International, Paper 730278, Jan. 1973.

[14] Miller, N. R., Shapiro, R., and McLaughlin, T. M., "A Technique for Obtaining Spatial Kinematic Parameters of Segments of Biomechanical Systems from Cinematographic Data," *Journal of Biomechanics*, Vol. 13, 1980, pp. 535–547. doi:10.1016/0021-9290(80)90054-8

[15] Mesqui, F., Niederer, P., Schlumpf, M., Lehareinger, Y., and Walton, J., "Semi-Automatic Reconstruction of the Spatial Trajectory of an Impacted Pedestrian Surrogate Using High-Speed Cinephotogrammetry and Digital Image Analysis," *Journal of Biomechanical Engineering*, Vol. 106, Nov. 1984, pp. 357–359.

[16] Mikhail, E. M., Bethel, J. S., and McGlone, J. C., *Introduction to Modern Photogrammetry*, Wiley, New York, 2001.

[17] Pappa, R. S., Giersch, L. R., and Quagloaroli, J. M., "Photogrammetry of a 5 m Inflatable Space Antenna with Consumer Digital Cameras," NASA TM-2000-210627, Dec. 2000.

[18] Ma, N., "The Study of Excimer Laser Beam Profile, Homigenizer's Beam Shaping Effect, and Fabrication of Reflective Thin Film Test Articles," M.S. Thesis, Dept. of Electrical and Computer Engineering, Univ. of Kentucky, Lexington, KY, Dec. 2004.

G. Agnes
Associate Editor